Detailed theoretical investigation of bending properties in solid-core photonic bandgap fibers

Tadashi Murao, Kunimasa Saitoh, and Masanori Koshiba

Graduate School of Information Science and Technology, Hokkaido University, Sapporo 060-0814, Japan
murao@icp.ist.hokudai.ac.jp

Abstract: In this paper, detailed properties of bent solid-core photonic bandgap fibers (SC-PBGFs) are investigated. We propose an approximate equivalent straight waveguide (ESW) formulation for photonic bandgap (PBG) edges, which is convenient to see qualitatively which radiation (centripetal or centrifugal radiation) mainly occurs and the impact of bend losses for an operating wavelength. In particular, we show that cladding modes induced by bending cause several complete or incomplete leaky mode couplings with the core mode and the resultant loss peaks. Moreover, we show that the field distributions of the cladding modes are characterized by three distinct types for blue-edge, mid-gap, and red-edge wavelengths in the PBG, which is explained by considering the cladding Bloch states or resonant conditions without bending. Next, we investigate the structural dependence of the bend losses. In particular, we demonstrate the bend-loss dependence on the number of the cladding rings. Finally, by investigating the impacts of the order of PBG and the core structure on the bend losses, we discuss a tight-bending structure.

OCIS codes: (060.2280) Fiber design and fabrication; (060.2310) Fiber optics; (060.2400) Fiber properties; (060.5295) Photonic crystal fibers.

References and links

1. J. C. Knight, F. Luan, G. J. Pearce, A. Wang, T. A. Birks, and D. M. Bird, "Solid photonic bandgap fibres and applications," Jpn. J. Appl. Phys. **45**, 6059-6063 (2006).
2. R. F. Cregan, B. J. Mangan, J. C. Knight, T. A. Birks, P. S. J. Russell, P. J. Roberts, and D. C. Allan, "Single-mode photonic band gap guidance of light in air," Science **285**, 1537-1539 (1999).
3. J. C. Knight, "Photonic crystal fibres," Nature **424**, 847-851 (2003).
4. T. Murao, K. Saitoh, and M. Koshiba, "Design of air-guiding modified honeycomb photonic band-gap fibers for effectively single-mode operation," Opt. Express **14**, 2404-2412 (2006).
5. R. Amezcua-Correa, N. G. R. Broderick, M. N. Petrovich, F. Poletti, and D. J. Richardson, "Optimizing the usable bandwidth and loss through core design in realistic hollow-core photonic bandgap fibers," Opt. Express **14**, 7974-7985 (2006).
6. F. Benabid, "Hollow-core photonic bandgap fibre: new light guidance for new science and technology," Phil. Trans. R. Soc. A **364**, 3439-3462 (2006).
7. T. Murao, K. Saitoh, and M. Koshiba, "Structural optimization of air-guiding photonic bandgap fibers for realizing ultimate low loss waveguides," J. Lightwave Technol. **26**, 1602-1612 (2008).
8. N. M. Litchinitser, S. C. Dunn, B. Usner, B. J. Eggleton, T. P. White, R. C. McPhedran, and C. M. de Sterke, "Resonances in microstructured optical waveguides," Opt. Express **11**, 1243-1251 (2003).
9. J. Lægsgaard, "Gap formation and guided modes in photonic bandgap fibres with high-index rods," J. Opt. A **6**, 798-804 (2004).
10. T. A. Birks, D. M. Bird, T. D. Hedley, J. M. Pottage, and P. St. J. Russell, "Scaling laws and vector effects in bandgap-guiding fibres," Opt. Express **12**, 69-74 (2004).
11. F. Couny, F. Benabid, P. J. Roberts, M. T. Burnett, and S. A. Maier, "Identification of Bloch-modes in hollow-core photonic crystal fiber cladding," Opt. Express **15**, 325-338 (2007).
12. M. A. Duguay, Y. Kokubun, T. L. Koch, and L. Pfeiffer, "Antiresonant reflecting optical waveguides in SiO_2-Si multilayer structures," Appl. Phys. Lett. **49**, 13-15 (1986).
13. K. J. Rowland, S. Afshar V., and T. M. Monro, "Bandgaps and antiresonances in integrated-ARROWs and Bragg fibers; a simple model," Opt. Express **16**, 17935-17951 (2008).

#108481 - $15.00 USD Received 9 Mar 2009; revised 16 Apr 2009; accepted 19 Apr 2009; published 23 Apr 2009

14. P. Steinvurzel, B. T. Kuhlmey, T. P. White, M. J. Steel, C. M. de Sterke, and B. J. Eggleton, "Long wavelength anti-resonant guidance in high index inclusion microstructured fibers," Opt. Express **12**, 5424-5433 (2004).
15. F. Luan, A. K. George, T. D. Hedley, G. J. Pearce, D. M. Bird, J. C. Knight, and P. St. J. Russell, "All-solid photonic bandgap fiber," Opt. Lett. **29**, 2369-2371 (2004).
16. A. Argyros, T. A. Birks, S. G. Leon-Saval, C. M. B. Cordeiro, F. Luan, and P. St. J. Russell, "Photonic bandgap with an index step of one percent," Opt. Express **13**, 309-314 (2005).
17. T. T. Larsen, A. Bjarklev, D. S. Hermann, and J. Broeng, "Optical devices based on liquid crystal photonic bandgap fibres," Opt. Express **11**, 2589-2596 (2003).
18. N. M. Litchinitser, S. C. Dunn, P. E. Steinvurzel, B. J. Eggleton, T. P. White, R. C. McPhedran, and C. M. de Sterke, "Application of an ARROW model for designing tunable photonic devices," Opt. Express **12**, 1540-1550 (2004).
19. T. T. Alkeskjold, J. Lægsgaard, A. Bjarklev, D. S. Hermann, Anwatti, J. Broeng, J. Li, and S. Wu, "All-optical modulation in dye-doped nematic liquid crystal photonic bandgap fibers," Opt. Express **12**, 5857-5871 (2004).
20. M. W. Haakestad, T. T. Alkeskjold, M. D. Nielsen, L. Scolari, J. Riishede, H. E. Engan, and A. Bjarklev, "Electrically tunable photonic bandgap guidance in a liquid-crystal-filled photonic crystal fiber," IEEE Photon. Technol. Lett. **17**, 819-821 (2005).
21. T. T. Alkeskjold and A. Bjarklev, "Electrically controlled broadband liquid crystal photonic bandgap fiber polarimeter," Opt. Lett. **32**, 1707-1709 (2007).
22. A. Wang, A. K. George, and J. C. Knight, "Three-level neodymium fiber laser incorporating photonic bandgap fiber," Opt. Lett. **31**, 1388-1390 (2006).
23. T. Taru, J. Hou, and J. C. Knight, "Raman gain suppression in all-solid photonic bandgap fiber," in *proceedings of 2007 European Conference on Optical Communication (ECOC)*, 7.1.1 (2007).
24. C. B. Olausson, C. I. Falk, J. K. Lyngsϕ, B. B. Jensen, K. T. Therkildsen, J. W. Thomsen, K. P. Hansen, A. Bjarklev, and J. Broeng, "Amplification and ASE suppression in a polarization-maintaining ytterbium-doped all-solid photonic bandgap fibre," Opt. Express **16**, 13657-13662 (2008).
25. A. Argyros, T. A. Birks, S. G. Leon-Saval, C. M. B. Cordeiro, and P. St. J. Russell, "Guidance properties of low-contrast photonic bandgap fibres," Opt. Express **13**, 2503-2511 (2005).
26. T. A. Birks, F. Luan, G. J. Pearce, A. Wang, J. C. Knight, and D. M. Bird, "Bend loss in all-solid bandgap fibres," Opt. Express **14**, 5688-5698 (2006).
27. V. Pureur, A. Bétourné, G. Bouwmans, L. Bigot, M. Douay, and Y. Quiquempois, "Bending Losses in all solid 2D photonic band-gap fibers: a limiting factor?," in *proceedings of 2006 European Conference on Optical Communication (ECOC)*, We.P3.34 (2006).
28. J. M. Stone, G. J. Pearce, F. Luan, T. A. Birks, J. C. Knight, A. K. George, and D. M. Bird, "An improved photonic bandgap fiber based on an array of rings," Opt. Express **14**, 6291-6296 (2006).
29. A. Bétourné, V. Pureur, G. Bouwmans, Y. Quiquempois, L. Bigot, M. Perrin, and M. Douay, "Solid photonic bandgap fiber assisted by an extra air-clad structure for low-loss operation around 1.5 μm," Opt. Express **15**, 316-324 (2007).
30. A. Bétourné, G. Bouwmans, Y. Quiquempois, M. Perrin, and M. Douay, "Improvements of solid-core photonic bandgap fibers by means of interstitial air holes," Opt. Lett. **32**, 1719-1721 (2007).
31. K. Kakihara, N. Kono, K. Saitoh, and M. Koshiba, "Full-vectorial finite element method in a cylindrical coordinate system for loss analysis of photonic wire bends," Opt. Express **14**, 11128-11141 (2006).
32. N. W. Ashcroft and N. D. Mermin, *Solid state physics,* (Holt, Rinehart, and Winston, 1976).
33. M. Perrin, Y. Quiquempois, G. Bouwmans, and M. Douay, "Coexistence of total internal reflection and bandgap modes in solid core photonic bandgap fibre with interstitial air holes," Opt. Express **15**, 13783-13795 (2007).
34. T. A. Birks, G. J. Pearce, and D. M. Bird, "Approximate band structure calculation for photonic bandgap fibres," Opt. Express **14**, 9483-9490 (2006).
35. G. Bouwmans, L. Bigot, Y. Quiquempois, F. Lopez, L. Provino, and M. Douay, "Fabrication and characterization of an all-solid 2D photonic bandgap fiber with a low-loss region (< 20 dB/km) around 1550 nm," Opt. Express **13**, 8452-8459 (2005).
36. M. J. F. Digonnet, H. K. Kim, G. S. Kino, and S. Fan, "Understanding air-core photonic-bandgap fibers: Analogy to conventional fibers," J. Lightwave Technol. **23**, 4169-4177 (2005).
37. Y. Li, C. Wang, T. A. Birks, and D. M. Bird, "Effective index method for all-solid photonic bandgap fibres," J. Opt. A **9**, 858-861 (2007).
38. J. Olszewski, M. Szpulak, and W. Urbańczyk, "Effect of coupling between fundamental and cladding modes on bending losses in photonic crystal fibers," Opt. Express **13**, 6015-6022 (2005).
39. Z. Zhang Y. Shi, B. Bian, and J. Lu, "Dependence of leaky mode coupling on loss in photonic crystal fiber with hybrid cladding," Opt. Express **16**, 1915-1922 (2008).

#108481 - $15.00 USD Received 9 Mar 2009; revised 16 Apr 2009; accepted 19 Apr 2009; published 23 Apr 2009

1. Introduction

Photonic bandgap fibers (PBGFs), classified in two categories, namely, the solid-core [1] and the air-core structure [2-7], guide light along the fiber length in the low-index defected core region by the photonic bandgap (PBG) effect because the cladding is usually made of periodically arranged two or three different index materials. Recently, researches have made progress in understanding the close relation between the PBG for light with out-of-plane propagation in solid-core photonic bandgap fibers (SC-PBGFs) [8,9], or in air-core structures (but rather more subtle [10,11]), and the theory for anti-resonant reflecting optical waveguides (ARROWs) [12,13]. Anti-resonant reflection reaches the minimum value for an operating wavelength λ in which high-index rods in the cladding satisfy the modal cutoff condition, when the rods are considered as "index-guiding waveguides" individually (resonant condition inside rods for perpendicular direction to the propagation axis at an effective index corresponding to the refractive index of low-index glass, where the ARROW mode's effective index must be near that value). On the other hand, the reflection reaches the maximum value in the wavelength range which satisfies the anti-resonant condition in rods, thus the SC-PBGFs support core modes at the defect.

Usually, the SC-PBGFs are realized by infiltrating high-index fluids such as liquid crystals into air holes of index-guiding photonic crystal fibers (PCFs) [14], or by periodically arranging Ge-doped rods in silica [15,16]. The former is expected to realize multiple useful devices such as an electrically or thermally tunable filter and polarimeter by externally applying an electric field or changing the temperature of the liquid crystals [17-21]. The latter, on the other hand, can be applied to selection of lasing transition in fiber lasers [22], suppression of Raman gain for the high-power laser delivery [23], and suppression of amplified spontaneous emission in fiber amplifiers [24], taking advantage of its fiber-type functionality of alternate transmission and transmission-inhibited bands.

Recently, bend losses in SC-PBGFs have attracted much attention because they might be one of the candidates for limiting its potentials [25-30]. It has been reported experimentally that the centripetal radiation as well as the centrifugal radiation occurs, when the fiber is bent, at longer wavelength ranges in the PBG [26]. This anomalous property was explained by considering the existence of the inner radiation caustic, based on the concept of the leaning of PBG edges, which can not be seen in conventional optical fibers [25,26]. However, a further analysis is required to understand the detailed properties of bent SC-PBGFs.

In this paper, we investigate the bending-loss properties for the SC-PBGFs through a full-vector modal solver based on the finite element method (FEM) with the cylindrical coordinate system [31]. We show numerically, for the first time, that the PBG edges lean with respect to the fiber cross section, which demonstrates the validity of the assumption that was proposed in [25,26] to explain the cause of the centripetal radiation in SC-PBGFs. In addition, we propose an approximate equivalent straight waveguide (ESW) formulation for PBG edges, which is convenient to see qualitatively which radiation (centripetal or centrifugal radiation) mainly occurs [26] and the impact of bend losses for an operating wavelength. In particular, we show that cladding modes induced by the bend cause several complete or incomplete leaky mode couplings with the core mode and the resultant loss peaks. Moreover, we show that the field distributions of the cladding modes are characterized by three distinct types for blue-edge, mid-gap, and red-edge wavelengths in the PBG. We explain that the distinct characteristics of the distributions can be understood by considering the cladding Bloch states or resonant conditions without bending. Next, we investigate the structural dependence of the bend losses. In particular, we show that the bending radius at which the bend loss increases drastically has no dependence on the number of the cladding rings, which is very crucial parameter in confinement losses. Moreover, it is shown that the bending radius value at the coupling points between the core and cladding modes has dependence on the number of the cladding rings for red-edge wavelength but no dependence for blue-edge and mid-gap wavelengths. Finally, by investigating the impacts of the order of PBG and the core structure on the bend losses, we discuss a tight-bending structure.

#108481 - $15.00 USD Received 9 Mar 2009; revised 16 Apr 2009; accepted 19 Apr 2009; published 23 Apr 2009

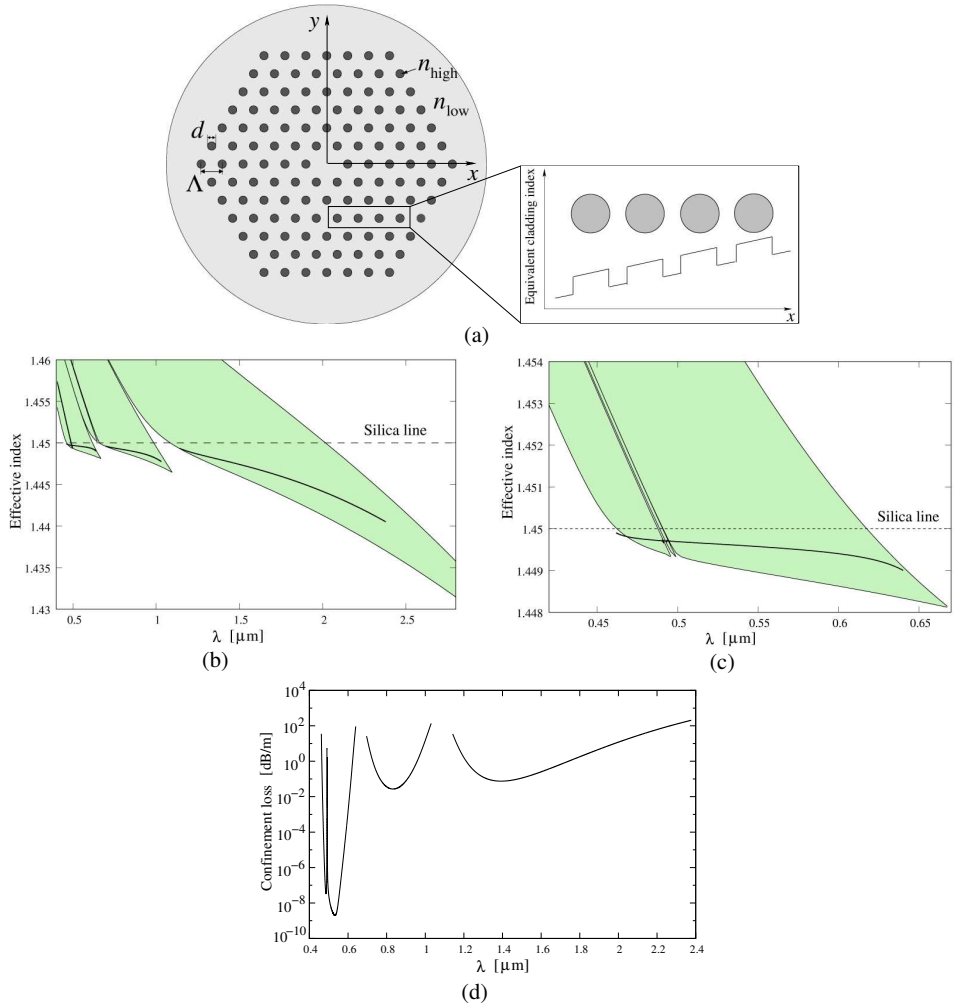

Fig. 1. (a) Cross section of SC-PBGF, where d stands for diameter of high-index rods, Λ for distance between adjacent rods, n_{high} for refractive index of high-index rods, and n_{low} for that of low-index background. Inset shows schematic equivalent index profile by approximate ESW formulation with bending of the fiber. (b) Dispersion curves of the fundamental mode of this fiber for the 1st to 3rd PBGs and (c) for the 3rd PBG with enlarged illustration, respectively, where the green color corresponds to the PBG region and the black dashed line to the silica-core index. (d) Confinement losses as a function of wavelength for the SC-PBGF with d/Λ = 0.4, Λ = 6.75 μm, n_{high} = 1.48, n_{low} = 1.45, and 6 cladding rings, respectively.

2. Fundamental properties of bent SC-PBGFs

Figure 1(a) shows the cross section of the SC-PBGF, whose cladding is composed of a periodic arrangement of high-index rods in a low-index background, where d stands for the diameter of the high-index rods, Λ is the distance between adjacent rods, and n_{high}, n_{low} are the refractive indices of the high-index rods and the low-index background, respectively. We set the origin coordinate at the central fiber cross section, x as the horizontal axis and y as the vertical axis, respectively, as in Fig. 1(a). As one of the common SC-PBGFs, unless otherwise specified, we choose the structural parameters as d/Λ = 0.4 and Λ = 6.75 μm, the core region is formed by removing 1 rod, and the number of cladding rings is 6, respectively (if another structure is considered, this will be the basis for comparison). The high-index rods of n_{high} = 1.48 in the silica background of n_{low} = 1.45 are realized by a Ge-doping or an infiltration of

#108481 - $15.00 USD Received 9 Mar 2009; revised 16 Apr 2009; accepted 19 Apr 2009; published 23 Apr 2009

the high-index liquid in air holes. (The frequency dependence of refractive indices is neglected because it is known that this has no significant impact on the results [26], while it may cause a small amount of wavelength shift.) In Figs. 1(b) and (c), we show the dispersion curves of the fundamental mode of this fiber for the 1st to 3rd PBGs in (b) and for the 3rd PBG with enlarged illustration in (c), respectively, calculated by using FEM, where the green color corresponds to the PBG region and the black dashed line to the silica-core index. The fundamental core mode exists in the PBG region. In solid-state physics, it is well known that, in a periodic potential, energy states split and energy gaps are generated at the Brillouin zone boundary due to the fact that the wavenumber of an electron in a periodic potential satisfies an arbitrary value of integral multiples of the reciprocal lattice [32]. In an analogous fashion, PBG edges in the SC-PBGF cladding always correspond to the transverse Brillouin zone boundary (in particular, high symmetry points [33]). In the resonant condition between PBG edges, a permitted band (namely, photonic band) is formed by an overlap of the rod modes which come from the resonance in high-index rods [9]. The width of the photonic band is increased when the overlap of the tight-binding rod modes increases; in other words, the coupling coefficient between the rod modes is increased [9,34], which is analogous to the tight-binding theory in solid-state physics. The upper edges of photonic bands are composed of coupled super modes with even states of the rod mode, while lower edges of photonic bands are composed of those with odd states [34], where the behavior is similar to two weakly coupled single-mode waveguides and also can be explained by using the Bloch theorem because these edges always correspond to the high symmetry points of the transverse Brillouin zone as mentioned above [33]. In general, the photonic band which resides between PBGs is associated with LP_{0m} or LP_{1m} mode of the rods because of the large overlap for these rod modes, while LP_{2m} mode (which nearly coincides with LP_{0m} mode), LP_{3m} and LP_{4m} modes of the rods (which occur between LP_{0m} and LP_{1m} modes) just get across the PBGs without spreading their width, despite the fact that the index-guiding rod modes already satisfy the cut-off condition below the silica line [9,26], where m is a nonnegative integer. In Fig. 1(d), we show the confinement losses as a function of wavelength for the 1st, 2nd and 3rd PBGs. Because the confinement losses at the lower order PBGs are effectively high due to the larger propagation angle of the guided modes, 3rd PBG is usually used [35]. We consider $\lambda = 0.471$ μm, 0.533 μm, and 0.62 μm as blue-edge, mid-gap and red-edge wavelengths, respectively, for the representative wavelengths in the 3rd PBG.

We consider the case that the SC-PBGF shown in Fig. 1(a) is bent leftward with a curvature radius of R. Because the equivalent refractive index profile of the bent fiber is determined by the approximate ESW formulation (see inset in Fig. 1(a)), expressed as

$$n_{eq}(x, y) = n(x, y)(1 + x/R), \tag{1}$$

where n represents the refractive index of the fiber and n_{eq} represents the equivalent refractive index with fiber bending, the photonic crystal cladding does not exhibit a periodicity for the fiber cross section, which results in a destruction of the concept of the PBG. According to the ARROW model, however, the principle of the confinement of light in the core region for the fiber with nonperiodic cladding can be understood by the overlaps of the anti-resonant conditions for the each high-index rod. When R decreases, on the other hand, the rods which do not satisfy the anti-resonant condition would be produced from the cladding edge. Accordingly, we can conclude that the "points" which do not satisfy the anti-resonant condition become "radiation caustics". If we impose the condition that the variations of the equivalent refractive indices for the each rod are effectively small, we can apply the idea of a "localized" PBG (variable PBG edge with a staircase for x) for this; that is, we replace the anti-resonant condition, which is somewhat ambiguous, with the bandgap condition (expressed with "edges"), which is strict in terms of the prohibit condition for penetration into the cladding. This idea leads to the concept of the "equivalent PBG-edge profile", proposed in [26]. Moreover, if we take the fact into account that the PBG edge can be interpreted as the refractive index of the cladding for step-index fibers in an analogy to conventional optical

#108481 - $15.00 USD Received 9 Mar 2009; revised 16 Apr 2009; accepted 19 Apr 2009; published 23 Apr 2009

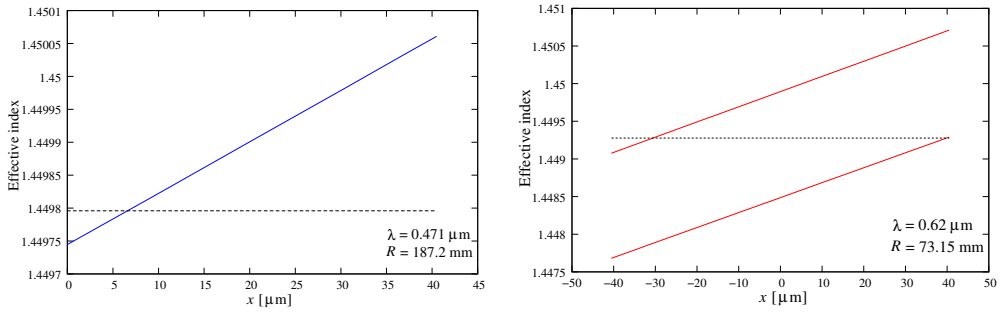

Fig. 2. Equivalent PBG edges as a function of x at the bend radius corresponding to the first appearance of the complete mode coupling (discussed in Fig. 3) for (a) blue-edge and (b) red-edge wavelengths, respectively.

Table 1. Comparison of results for gradient [1/μm] of PBG edges between FEM (in Fig. 2) and approximation (n_{edge}/R).

λ [μm]	R [mm]	FEM	approximation
0.471	187.2	7.81×10^{-6}	7.74×10^{-6}
0.62	73.15	2.02×10^{-5} (upper)	1.98×10^{-5} (upper)
		1.99×10^{-5} (lower)	1.98×10^{-5} (lower)

fibers because the PBG edge provides the condition with relation to the maximum (or minimum) permissible propagation angle for core modes in PBGFs [36,37], we can readily accept the concept of the "equivalent PBG-edge profile", which is analogous to the equivalent refractive index profile in conventional optical fibers.

Figures 2(a) and (b) show the equivalent PBG edges as a function of x, calculated by using FEM, for the blue-edge and red-edge wavelengths, respectively. The dashed line corresponds to the effective index of the guided mode. Only the alteration of the lower PBG edge is depicted for the blue-edge wavelength, while that of lower and higher PBG edges is depicted for the red-edge wavelength. We can see that the PBG edges practically lean with respect to the fiber cross section and the resultant outer radiation caustic exists for the blue-edge wavelength while the inner radiation caustic exists for the red-edge wavelength. We note that the equivalent cut-off V value for each rod which is expressed as

$$V_{eq} = (1 + x/R)V \,, \tag{2}$$

where

$$V = \pi d \sqrt{n_{high}^2 - n_{low}^2} \Big/ \lambda \,, \tag{3}$$

is nearly independent of bending because $R >> x$. Therefore, the wavelength which satisfies the antiresonant condition does not change for the rods in the fiber cross section. Moreover, because of this fact, the floor depth of a PBG relative to the equivalent low-index silica line (the floor depth is determined by the resonant condition in the low-index region [34]), is considered to have low variation with respect to x because the condition may be mainly associated with the size of the low-index region between the rods relative to wavelength. The effective index which satisfies the antiresonant condition (or "localized" PBG), however, does change with respect to x, which is the major factor for leaning of the PBG edges. We also note that the equivalent relative refractive index difference Δ_{eq} for each rod does not have any dependence on R and x when the Δ_{eq} is defined between the average indices of the diagonal high- and low-index profiles (inset of Fig. 1(a)), because of the following relationship:

#108481 - $15.00 USD Received 9 Mar 2009; revised 16 Apr 2009; accepted 19 Apr 2009; published 23 Apr 2009

$$\Delta_{eq}(x, y) = \frac{n_{high_{eq}}^2 - n_{low_{eq}}^2}{2n_{high_{eq}}^2} = \frac{n_{high}^2 - n_{low}^2}{2n_{high}^2} = \Delta \,, \tag{4}$$

where $n_{high_{eq}}$ and $n_{low_{eq}}$ stand for the equivalent index derived by the approximate ESW formulation (1), and Δ for the relative refractive index difference without bending. Because of the fact that the coupling coefficients between adjacent rod modes stay about the same for the rods with different x because both cut-off V_{eq} value and Δ_{eq} do not change with bending as mentioned above, the photonic-band width, which is determined by this coupling coefficient [34], does not affect the PBG edge condition itself when R decreases. Therefore, by considering these reasons, we can conclude that the equivalent PBG edges have dependence on the horizontal fiber cross section x, with a gradient equal to n_{edge}/R, where n_{edge} stands for the effective index of the PBG edge without bending. We compare the results by FEM (in Fig. 2) and this approximation in Table 1. We can clearly see the validity of this approximation. Therefore, the approximate ESW formulation for PBG edges is given by the same formula as that for the equivalent refractive index profiles,

$$n_{edge_{eq}}(x) = n_{edge}(1 + x/R) \,. \tag{5}$$

This formulation is convenient to see qualitatively which radiation (centripetal or centrifugal radiation) mainly occurs [26] and the impact of bend losses for an operating wavelength, as discussed later.

In Figs. 3(a)-(c), we show the bend-radius dependence of the effective refractive indices of the modes for the blue-edge, mid-gap, and red-edge wavelengths, respectively. When the bend radius is effectively small, several couplings occur between the fundamental and cladding modes as can be seen in index-guiding PCFs [38]. In Figs. 4(a)-(c), we depict the x-component of the electric field distributions of the horizontally polarized modes at the bend radius corresponding to the first appearance of the complete mode coupling for the blue-edge, mid-gap, and red-edge wavelengths, respectively. It is noted that the rod modes induced by bending are related to the LP super modes constructing the photonic bands in the cladding which the effective index line of the guided mode crosses in Fig. 2, as reported experimentally [26]. The rod modes consist of LP_{12} mode for the blue-edge and mid-gap, and LP_{02} mode for the red-edge wavelength, respectively. We also note that the cladding modes for the blue-edge and mid-gap wavelengths exist at the outer cladding with respect to the bent direction, which is similar to the case for the index-guiding PCFs [38], because of the existence of the outer radiation caustic as can be seen in Fig. 2(a). On the other hand, the modes for the red-edge wavelength exist at the inner cladding with respect to the bent direction because of the existence of the inner radiation caustic as can be seen in Fig. 2(b), contrary to the index-guiding case. If we look to the Fig. 4, in addition to the differences in terms of the centrifugal and centripetal radiation, we can clearly see that the characteristics of the distributions of the cladding modes for each wavelength are quite different; that is, the intensity of the electric field between rods is high for the blue-edge while being low for the red-edge and strongly localized for the mid-gap wavelength. We explain this phenomenon by considering the cladding Bloch states or resonant conditions without bending. Photonic bands which reside between PBGs are formed due to the coupling between tight-binding rod modes in the cladding [9,34]. At a blue edge of a PBG, the coupling state between two arbitrary rods is even, while at a red edge of a PBG the state is odd [34], which can be understood by the Bloch state in the cladding [33]. Because this tendency does not change drastically when SC-PBGFs are bent due to the small variation of the equivalent refractive index profile in the cladding, the intensity of the electric field of the modes between rods becomes non-zero at the blue-edge wavelength and zero at the red-edge wavelength. For the mid-gap wavelength, on the other hand, because the floor of a PBG is determined by the resonant condition in the low-index region [34], the field is strongly localized between rods. In Fig. 5, we show the bend

#108481 - $15.00 USD Received 9 Mar 2009; revised 16 Apr 2009; accepted 19 Apr 2009; published 23 Apr 2009

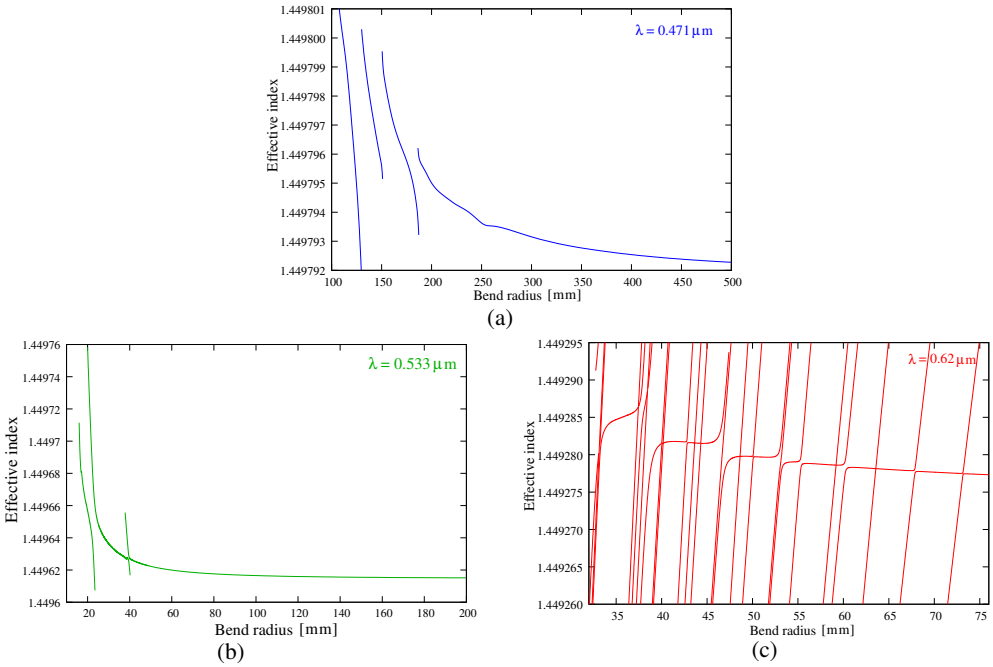

Fig. 3. Bend-radius dependence of the effective refractive indices of the modes for the (a) blue-edge, (b) mid-gap, and (c) red-edge wavelengths, respectively.

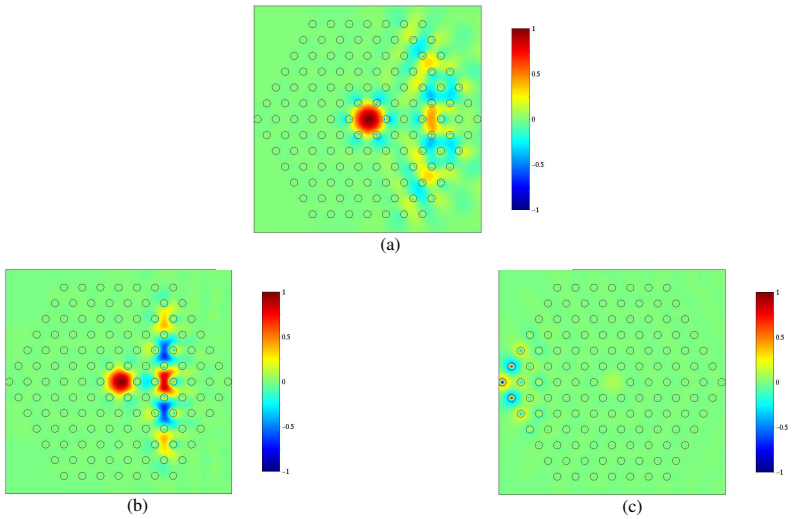

Fig. 4. *x*-component of electric field distributions of horizontally polarized modes at the bend radius corresponding to the first appearance of the complete mode coupling (in Fig. 3) for the (a) blue-edge, (b) mid-gap, and (c) red-edge wavelengths, respectively. The rod modes consist of LP_{12} mode for blue-edge and mid-gap, and LP_{02} mode for red-edge wavelength, respectively.

losses as a function of the bend radius for the blue-edge and red-edge wavelengths in (a), and for the mid-gap and red-edge wavelengths in (b), respectively. The bend loss for the blue-edge wavelength becomes increasingly high with the decrement of the bend radius, which agrees with the experimental result in [26]. This is because the effective index of the PBG edge exists near that of the core mode for the blue-edge wavelength [26]; more precisely, due to this fact, the resultant radiation caustic is supposed to reside near the core as in Fig. 2(a). It is noted

#108481 - $15.00 USD Received 9 Mar 2009; revised 16 Apr 2009; accepted 19 Apr 2009; published 23 Apr 2009

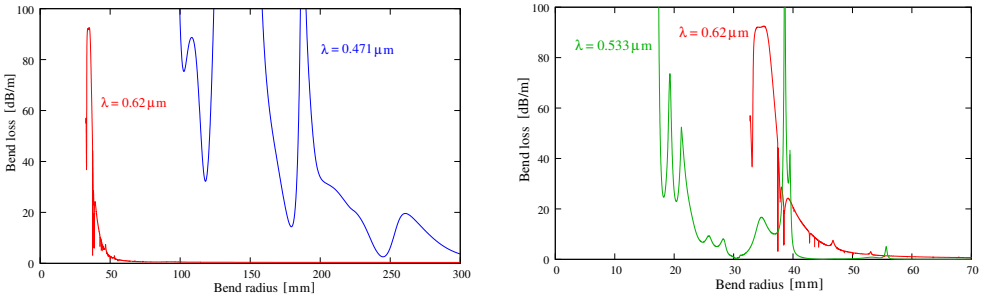

Fig. 5. Bend losses as a function of bend radius for (a) blue-edge and red-edge wavelengths, and for (b) mid-gap and red-edge wavelengths, respectively.

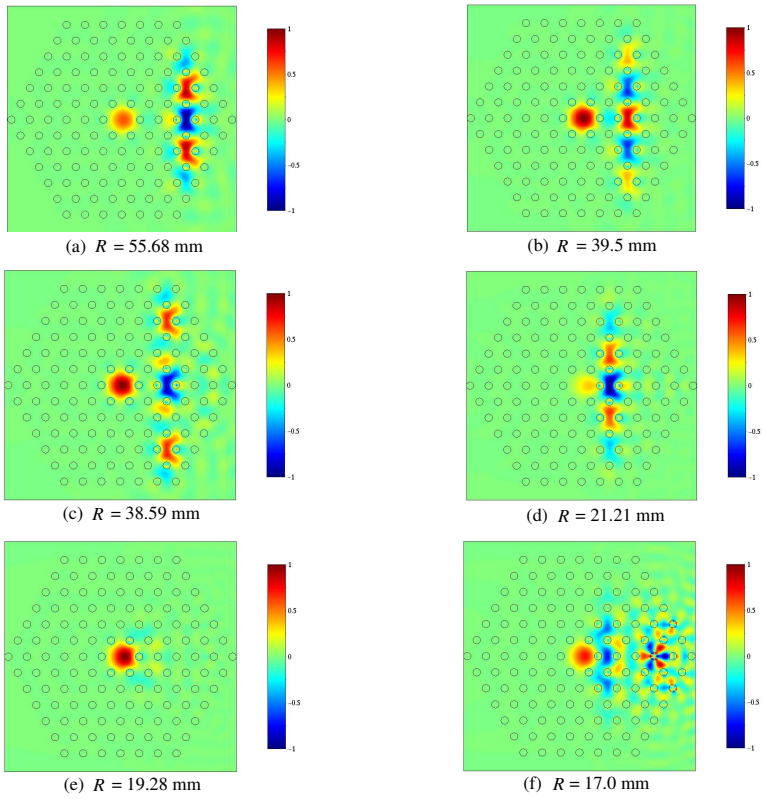

Fig. 6. *x*-component of the electric field distributions of the horizontally polarized modes at the loss peaks (in Fig. 5(b)) due to mode coupling between core and cladding modes for mid-gap wavelength.

that, if we look to the bend losses for the blue-edge and mid-gap wavelengths, we can see that the cladding modes induced by the bend cause the several high loss peaks. Some of them correspond to the anti-crossing points in Fig. 3; on the other hand, others do not correspond to such points, but to slight changes in the real part of the effective indices at the corresponding bend radii. This can be interpreted as the incomplete leaky mode coupling because of the large differences of the imaginary parts of the effective indices between the core and the cladding modes relative to the coupling coefficient [39]. We also note that though the bend losses of the cladding modes for the blue-edge and mid-gap wavelengths are higher than that of the core mode, most of those for the red-edge wavelength are, on the other hand, lower than that

#108481 - $15.00 USD Received 9 Mar 2009; revised 16 Apr 2009; accepted 19 Apr 2009; published 23 Apr 2009

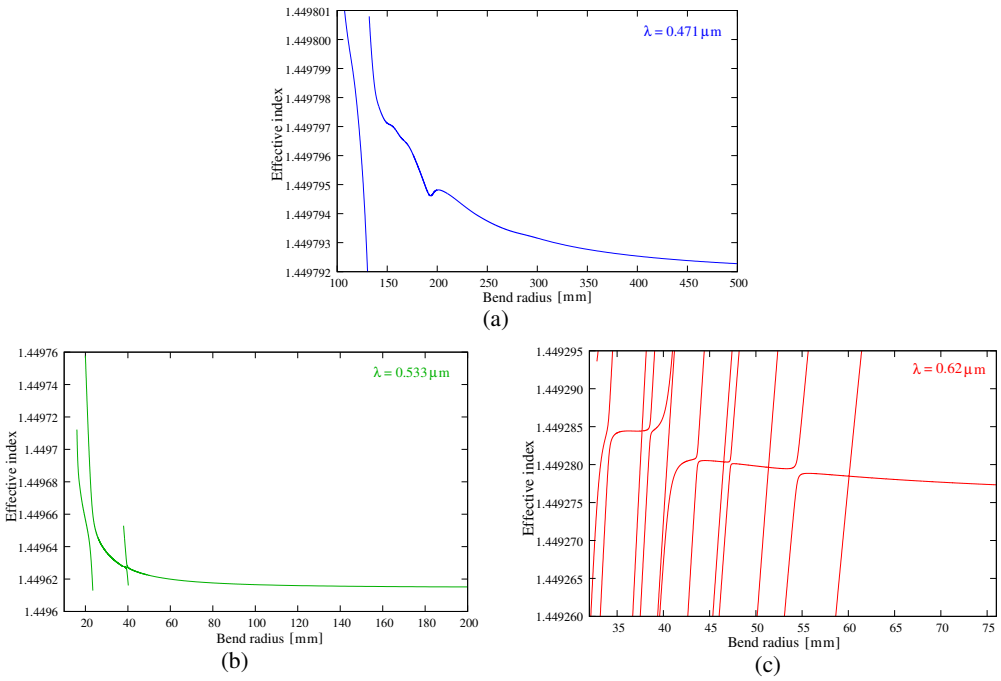

Fig. 7. Bend-radius dependence of the effective refractive indices of the modes for the fiber with 5 cladding rings for the (a) blue-edge, (b) mid-gap, and (c) red-edge wavelengths, respectively.

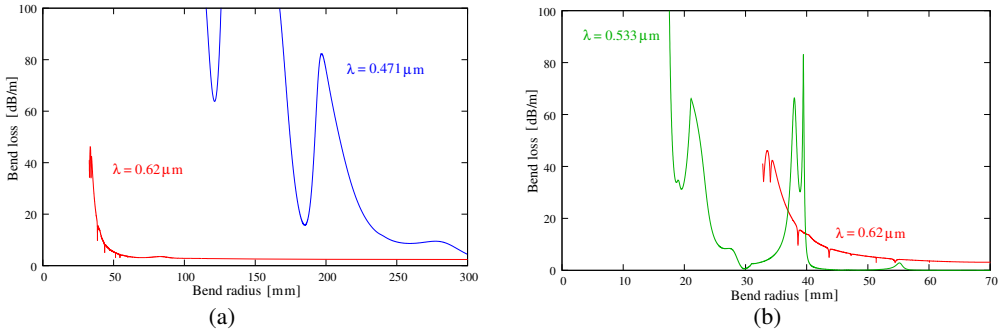

Fig. 8. Bend losses as a function of bend radius for the fiber with 5 cladding rings for (a) blue-edge and red-edge wavelengths, and for (b) mid-gap and red-edge wavelengths, respectively.

of the core mode. For this reason, the cladding modes for the red-edge wavelength do not contribute to the loss peaks in Fig. 5. Next, we demonstrate the transition of the cladding modes at the loss peaks for the mid-gap wavelength (because the field distributions for the blue-edge and red-edge wavelengths are too complicated, we show those only for the mid-gap wavelength). In Figs. 6(a)-(f), we depict the *x*-component of the electric field distributions of the horizontally polarized modes at the loss peaks (in Fig. 5(b)) due to mode coupling between the core and cladding modes for the mid-gap wavelength. For the SC-PBGFs with 6 cladding rings, there exist 5 columns of the low-index regions between rods on *x*-axis from the core to the outside of the photonic crystal region. When R decreases and bend radius attains to R = 55.68 mm, the core mode is coupled to the cladding mode localized at the 3rd column of the low-index regions between rods from the outside of the photonic crystal region. Because decreasing of the bend radius leads to a large gradient of the effective PBG edge,

#108481 - $15.00 USD Received 9 Mar 2009; revised 16 Apr 2009; accepted 19 Apr 2009; published 23 Apr 2009

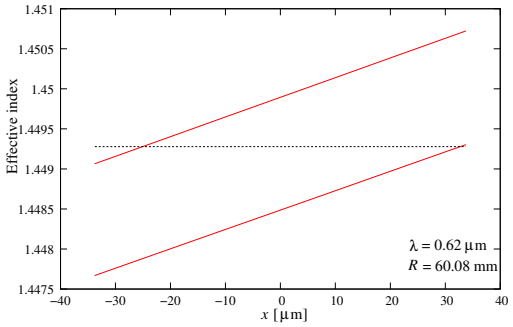

Fig. 9. Equivalent PBG edges as a function of x at the bend radius corresponding to the first appearance of the complete mode coupling (in Fig. 7(c)) for the red-edge wavelength.

which results in the approach of the radiation caustic to the core, the cladding mode coupling to the core mode also comes close to the core as seen in Figs. 6 (a)-(f). When the bend radius attains to R = 17.0 mm, we can see the excitation of the LP_{31} mode as well as the LP_{12} mode in the rod modes.

3. Structural, wavelength, and order of PBG dependence of bend losses

We investigate the characteristics of the bent SC-PBGFs as a function of the number of the cladding rings. In Fig. 7, we present the bend-radius dependence of the effective refractive indices of the modes for the structure with 5 cladding rings for the (a) blue-edge, (b) mid-gap, and (c) red-edge wavelengths, respectively, while in Fig. 8 we show the bend losses for the blue-edge and red-edge wavelengths in (a), and for the mid-gap and red-edge wavelengths in (b), respectively. The fluctuations in the effective index (in Fig. 7) accompanied by the loss peaks (in Fig. 8) are due to the incomplete leaky mode coupling because of the large difference of the imaginary parts between the core and cladding modes. It is worth noting that the critical bend radius below which the bend loss increases drastically is independent of the number of cladding rings though this is very crucial parameter in confinement losses. We also notice that the bend radii for which the cladding modes induced by the bend appear shift to smaller values for the red-edge wavelength, as compared with Fig. 3(c). This is because the reduction of the cladding area causes the necessary requirement to decrease the bend radius for the presence of the radiation caustic, as shown in Fig. 9. Although this phenomenon is also seen in the results for the blue-edge and mid-gap wavelengths, it seems that the bending radius value at the coupling points has no dependent on the number of cladding rings for these wavelengths. The reason for this is that, because the imaginary parts of effective indices of the cladding modes for the blue-edge and mid-gap wavelengths are larger than that for the red-edge wavelength as mentioned above, the mode coupling between the core and the cladding mode does not occur due to the large incompleteness of the leaky mode coupling for both of the fibers with 6 and 5 cladding rings when the bend radius is large (in this case, the radiation caustic is far from the core; in other words, the coupling coefficient is low). In addition to this fact, when the bend radius is small (in other words, the radiation caustic is near the core), because of the fact that the alignment of the high-index rods around the core stays about the same even if the number of the cladding rings is changed, the couplings occur on the condition that the distance between the core and the radiation caustic is the same for these structures. As an example, in Figs. 10(a)-(e), we depict the x-component of the electric field distributions of the horizontally polarized modes at the loss peaks (in Fig. 8(b)) due to mode coupling between the core and cladding modes at the mid-gap wavelength for the fiber with 5 cladding rings. In this case, there exist 4 columns of the low-index regions between rods on x-axis from the core to the outside of the photonic crystal region. When R = 39.46 mm, the coupling occurs between the core and the cladding mode localized at the 3rd column of the low-index regions between rods from the outside of the photonic crystal region which corresponds to the case at R = 55.68 mm for the 6-cladding-rings fiber (see Fig. 6). This bend

#108481 - $15.00 USD Received 9 Mar 2009; revised 16 Apr 2009; accepted 19 Apr 2009; published 23 Apr 2009

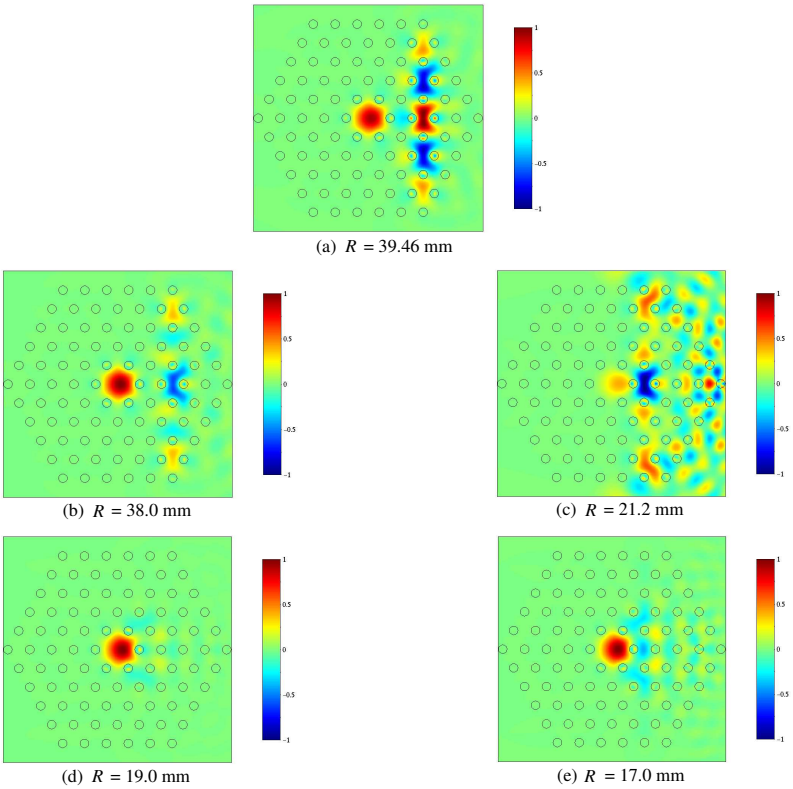

Fig. 10. x-component of the electric field distributions of the horizontally polarized modes at the loss peaks (in Fig. 8(b)) due to mode coupling between core and cladding modes for mid-gap wavelength for the 5-cladding-rings SC-PBGF with d/Λ = 0.4 and Λ = 6.75 μm (same as Fig. 6 except for the number of the cladding rings).

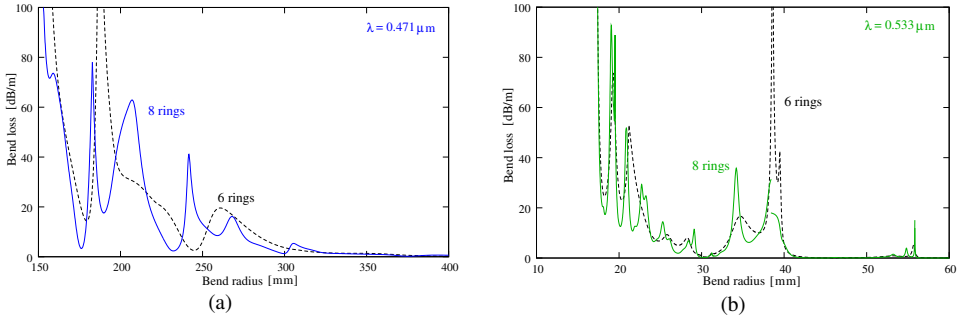

Fig. 11. Bend losses as a function of bend radius for the fiber with 8 cladding rings for (a) blue-edge and (b) mid-gap wavelengths. The bend losses for 6 cladding rings (shown in Fig. 5) are also shown with dotted curves as a reference.

radius for the 5-cladding-rings fiber is smaller than that for the 6-cladding-rings fiber as mentioned above. In this case, however, because the distance between the core and the region at which the cladding mode is localized is corresponding to the case at R = 39.5 mm for the 6-cladding-rings fiber, the bend radius stays about the same for Fig. 10(a) and Fig. 6(b).

We should comment on the concern that increment of the number of cladding rings may lead to the high bend losses due to the effect of cladding modes as mentioned in [29]. As an example, in Fig. 11 we present the bend losses as a function of the bend radius for the fiber with 8 cladding rings at the (a) blue-edge and (b) mid-gap wavelengths, respectively. We can

#108481 - $15.00 USD Received 9 Mar 2009; revised 16 Apr 2009; accepted 19 Apr 2009; published 23 Apr 2009

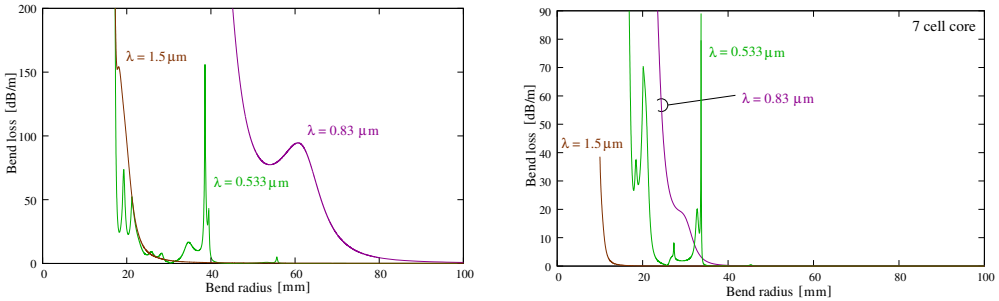

Fig. 12. Comparison of bend losses as a function of bend radius for the mid-gap wavelength of 1st, 2nd and 3rd PBGs for the structures with (a) 1 cell core and 6 cladding rings, and (b) 7 cell core and 5 cladding rings (cladding region is in keeping with that of the fiber with 1 cell core and 6 cladding rings).

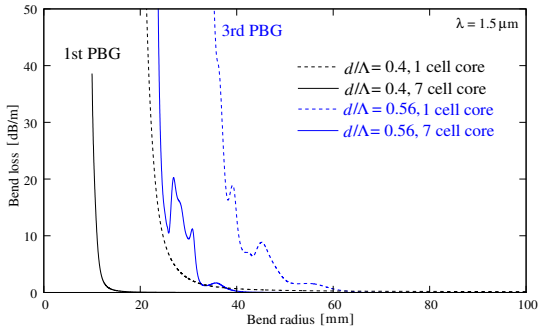

Fig. 13. Bend losses as a function of bend radius for the fibers with $d/\Lambda = 0.4$, $\Lambda = 6.75$ μm, 7 cell core and 5 cladding rings (solid black curve), and with $d/\Lambda = 0.56$, $\Lambda = 13.5$ μm, 1 cell core and 6 cladding rings (dashed blue curve) at $\lambda = 1.5$ μm (mid-gap wavelength of the fibers). The core radius relative to wavelength is almost identical for the fibers. As a reference, bend losses for the fibers with $d/\Lambda = 0.4$, $\Lambda = 6.75$ μm, 1 cell core and 6 cladding rings (dashed black curve), and with $d/\Lambda = 0.56$, $\Lambda = 13.5$ μm, 7 cell core and 5 cladding rings (solid blue curve) are also depicted at the same time.

clearly see that the bend losses oscillate for the variation of bend radius though the critical bend radius is still independent on the number of cladding rings. This oscillation may be caused by the following reason: A fiber with a large number of cladding rings supports additional cladding modes and also reduces the imaginary part of the effective index of the modes. Accordingly, leaky mode couplings between the core and cladding modes occur multiple times. In this case, the conservation of the bend radius at which cladding modes appear for changing of the number of cladding rings in the blue-edge and mid-gap wavelengths, as mentioned above, is not applicable.

Next, we investigate the order of PBG dependence of the bend losses for the SC-PBGFs. We consider $\lambda = 0.533$ μm, 0.83 μm, and 1.5 μm as the mid-gap wavelengths for the 3rd, 2nd, and 1st PBGs, respectively. Figure 12(a) shows the bend losses as a function of the bend radius at the mid-gap wavelengths of the 1st, 2nd and 3rd PBGs for the SC-PBGFs with 6 cladding rings. The bend loss for the 2nd PBG is comparatively high because the photonic band which resides between 2nd and 3rd PBGs consists of the coupling system of the LP_{02} rod modes [26]. Though the critical bend radius is almost the same for the 1st and 3rd PBGs, several bend-loss peaks exist for the 3rd PBG. In Fig. 12(b), we present the bend losses as a function of the bend radius at the mid-gap wavelengths for the SC-PBGFs with 7 cell core (the core is formed by removing 7 high-index rods) and 5 cladding rings (to keep the cladding region when compared to the fiber with 1 cell core and 6 cladding rings). The decrement of the propagation angle to the fiber axis of the core mode (in other words, increment of the

#108481 - $15.00 USD Received 9 Mar 2009; revised 16 Apr 2009; accepted 19 Apr 2009; published 23 Apr 2009

effective index) due to the enlargement of the core radius leads to the betterment of bending characteristics. In particular, it is worth noting that the critical bend radius for the 1st PBG is drastically reduced. This result is associated with the fact that the floor depth of 1st PBG is larger than that of 3rd PBG [26] and the large betterment of the decrement of the propagation angle for the 1st PBG.

Actually, in most situations, there is an issue; which structure has advantages in terms of low bend losses. In order to obtain the solution, it is required to compare structures having constant core radii relative to wavelength, by setting the operating wavelength and effective core area, because the elimination of the effect of the core radius on bending losses is important, and these values tend to be requested in advance in most situations. We investigate which order of PBGs has the advantage in terms of low bending losses (we assume the case that the value of Δ is constant). In Fig. 13, we show the bend losses as a function of the bend radius at λ = 1.5 μm for the fibers with d/Λ = 0.4, Λ = 6.75 μm, 7 cell core and 5 cladding rings (solid black curve) whose mid-gap wavelength of the 1st PBG is set at λ = 1.5 μm, and with d/Λ = 0.56, Λ = 13.5 μm, 1 cell core and 6 cladding rings (dashed blue curve) whose mid-gap wavelength of the 3rd PBG is set at λ = 1.5 μm. The core radius relative to wavelength is almost identical for these fibers (the cladding region is, however, quite different for these fibers because, in general, the use of 3rd PBG leads to thicker fibers due to the large pitch). As a reference, the bend losses for the fibers with d/Λ = 0.4, Λ = 6.75 μm, 1 cell core and 6 cladding rings (dashed black curve), and with d/Λ = 0.56, Λ = 13.5 μm, 7 cell core and 5 cladding rings (solid blue curve) are also depicted at the same time. We can clearly see that the critical bend radius for the structure using the 1st PBG with 7 cell core is smaller when compared to the structure using the 3rd PBG with 1 cell core (or even with 7 cell core). This result is associated with the fact that the floor depth of the 1st PBG is larger than that of the 3rd PBG as mentioned above. Actually, a 7-cell-core SC-PBGF, however, operates in multi-moded. In order to take advantage of this structure, there is a necessary requirement that the SC-PBGF operates in single-moded at the 1st PBG without degradation of the bending property such as a critical bend radius. We are now under constructing such a SC-PBGF and the concept of the totally novel SC-PBGF will be discussed elsewhere. Additional investigations for impacts of structural parameters on the bending losses are presented in the appendix.

4. Conclusions

In this work, the PBG-edges alteration with respect to the fiber cross section was numerically investigated, to the best of our knowledge, for the first time in bent SC-PBGFs. We have shown that the PBG edges lean with respect to the fiber cross section, which demonstrates the validity of the assumption that was proposed in [25,26] to explain the cause of the centripetal radiation in SC-PBGFs. We developed an approximate ESW formulation for PBG edges. We have shown that cladding modes induced by the bend cause several complete or incomplete leaky mode couplings with the core mode and the resultant loss peaks. Moreover, we have shown that the field distributions of the cladding modes are characterized by three distinct types for blue-edge, mid-gap, and red-edge wavelengths in the PBG, which can be understood by considering the cladding Bloch states or resonant conditions without bends. Next, we have investigated the structural dependence of the bend losses. In particular, we have shown that the bending radius at which the bend loss increases drastically has no dependence on the number of the cladding rings, though this is very crucial parameter in confinement losses. Moreover, it has been shown that the bending radius value at the coupling points between the core and cladding modes has dependence on the number of the cladding rings for red-edge wavelength but no dependence for blue-edge and mid-gap wavelengths. Finally, by investigating the impacts of the order of PBG and the core structure on the bend losses, we discussed a tight-bending structure.

#108481 - $15.00 USD Received 9 Mar 2009; revised 16 Apr 2009; accepted 19 Apr 2009; published 23 Apr 2009

Appendix – significance of structural parameters

In this work, we have considered the SC-PBGF with the particular structural parameters as the basis for comparison. Here, we demonstrate whether a determination of the pair for the value of d/Λ and Δ affects the bend losses or not. According to the ARROW theory [8], this pair should be chosen as satisfying the constant value of $(d/\Lambda)\times\sqrt{n_{high}^2 - n_{low}^2}$ if the order of operating PBG is invariant (we consider the case that Λ is constant). In Fig. 14, we show the pair (d/Λ, Δ) dependence of the bend losses for the mid-gap wavelength of the (a) 3rd PBG for the 1 cell-core structure, (b) 1st PBG for the 1 cell-core structure, and (c) 1st PBG for the 7 cell-core structure. In order to eliminate the effect of the core radius on bending losses, the core radius is constant relative to wavelength in each figure. We note that the critical bend radius is drastically changed by slightly varying the value of d/Λ and Δ, while the effective indices of the core modes without bending and the PBG edges for each core structure and wavelength remain almost the same (the differences are about 10^{-5} and 10^{-4}, respectively). This implies that, by selecting the appropriate value of the pair, an improvement of the bending properties is possible without changing the other fiber properties, though we believe the further investigation is needed to see this in detail. In addition to this, the investigation for the degree of accuracy of theoretical formula of Eq. (2) in Ref. [26] is also an issue in the future.

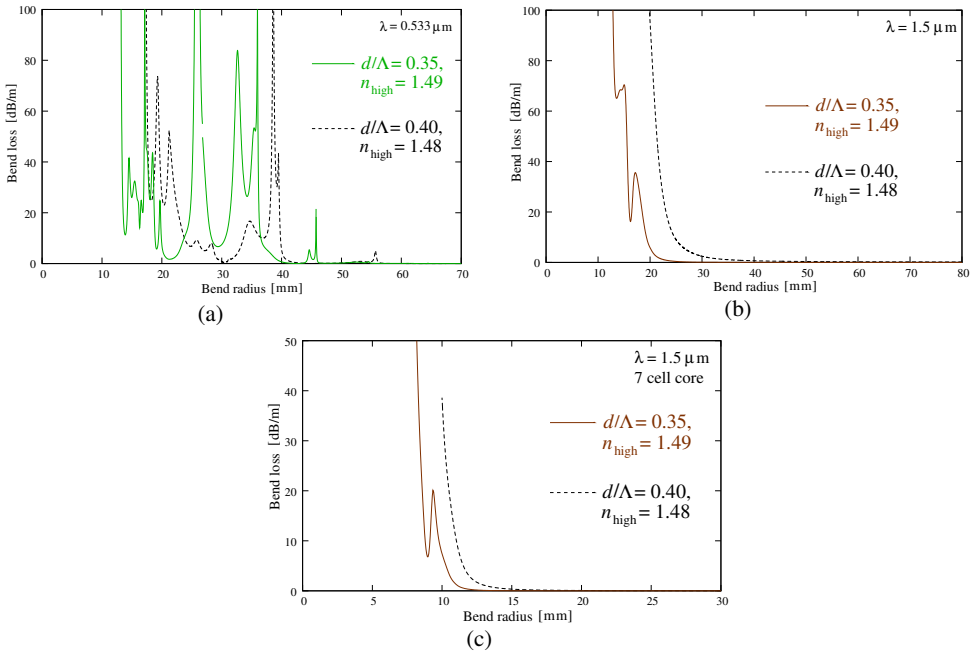

Fig. 14. Comparison of bend losses as a function of bend radius for the d/Λ = 0.4, n_{high} = 1.48 and d/Λ = 0.35, n_{high} = 1.49 at the mid-gap wavelength of (a) 3rd PBG for 1 cell-core structure, (b) 1st PBG for 1 cell-core structure, and (c) 1st PBG for 7 cell-core structure. The pitch for both structures is Λ = 6.75 μm.

Acknowledgments

The authors would like to kindly acknowledge the financial support of this project from the Japan Society for the Promotion of Science (JSPS), Grant-in-Aid for JSPS Fellows (20-2266). They are thankful to Dr. L. Rosa from Hokkaido University for stimulating discussions.

#108481 - $15.00 USD Received 9 Mar 2009; revised 16 Apr 2009; accepted 19 Apr 2009; published 23 Apr 2009